Fly cryptochrome and the visual system

Gabriella Mazzotta[a], Alessandro Rossi[a,b], Emanuela Leonardi[a], Moyra Mason[a], Cristiano Bertolucci[c], Laura Caccin[a], Barbara Spolaore[d], Alberto J. M. Martin[a], Matthias Schlichting[e], Rudi Grebler[e], Charlotte Helfrich-Förster[e], Stefano Mammi[b], Rodolfo Costa[a,1], and Silvio C. E. Tosatto[a]

[a]Department of Biology, University of Padova, 35131 Padova, Italy; [b]Department of Chemical Sciences, University of Padova, 35131 Padova, Italy; [c]Department of Life Science and Biotechnologies, University of Ferrara, 44121 Ferrara, Italy; [d]Centro Ricerche Interdipartimentale Biotecnologie Innovative, University of Padova, 35131 Padova, Italy; and [e]Neurobiology and Genetics, Biocenter, University of Würzburg, 97074 Würzburg, Germany

Edited by Jay C. Dunlap, Dartmouth Medical School, Hanover, NH, and approved February 25, 2013 (received for review July 18, 2012)

Cryptochromes are flavoproteins, structurally and evolutionarily related to photolyases, that are involved in the development, magnetoreception, and temporal organization of a variety of organisms. *Drosophila* CRYPTOCHROME (dCRY) is involved in light synchronization of the master circadian clock, and its C terminus plays an important role in modulating light sensitivity and activity of the protein. The activation of dCRY by light requires a conformational change, but it has been suggested that activation could be mediated also by specific "regulators" that bind the C terminus of the protein. This C-terminal region harbors several protein–protein interaction motifs, likely relevant for signal transduction regulation. Here, we show that some functional linear motifs are evolutionarily conserved in the C terminus of cryptochromes and that class III PDZ-binding sites are selectively maintained in animals. A coimmunoprecipitation assay followed by mass spectrometry analysis revealed that dCRY interacts with Retinal Degeneration A (RDGA) and with Neither Inactivation Nor Afterpotential C (NINAC) proteins. Both proteins belong to a multiprotein complex (the Signalplex) that includes visual-signaling molecules. Using bioinformatic and molecular approaches, dCRY was found to interact with Neither Inactivation Nor Afterpotential C through Inactivation No Afterpotential D (INAD) in a light-dependent manner and that the CRY–Inactivation No Afterpotential D interaction is mediated by specific domains of the two proteins and involves the CRY C terminus. Moreover, an impairment of the visual behavior was observed in fly mutants for dCRY, indicative of a role, direct or indirect, for this photoreceptor in fly vision.

Circadian clocks synchronize physiology and behavior of living organisms with 24-h environmental cycles. In *Drosophila*, the resetting of the clock depends mostly on light-mediated degradation of the clock protein TIMELESS (dTIM), which, in turn, affects the stability of its partner PERIOD (dPER). Light signals are received through the blue-light photoreceptor CRYPTOCHROME (dCRY), the expression of which is under clock control. dCRY associates with dTIM in a light-dependent manner and promotes its proteasome-mediated degradation (1). Cryptochromes are flavoproteins highly similar to photolyases, from which they have probably evolved, but across evolution they have lost or reduced the photolyase activity and gained roles in signaling (2). Cryptochromes consist of two protein domains: an N-terminal domain homologous to photolyases (Photolyase Related, or PHR), and a very divergent C-terminal tail (3). A class of cryptochromes, CRY-DASH (drosophila, arabidopsis, synechocystis, homo), with single-stranded DNA repair activity and without the C terminus tail, has been described in bacteria, plants, and animals (2). The role of cryptochromes in the circadian clock differs among the different species. Cryptochromes have merely a blue-light photoreceptor activity in plants whereas in mammals they are part of the central clock mechanism, and this function is not light dependent (4). In *Drosophila*, the unique CRY acts as a circadian photoreceptor in the master clock (5) whereas, in other insects, only the vertebrate-like CRYs play a role as transcriptional repressor (6). Moreover, dCRY has been shown to play a fundamental role in the fly's magnetosensitivity, i.e., the use of the Earth's magnetic field for orientation and navigation (7). dCRY is rhythmically expressed. Protein levels oscillate only under light–dark cycling conditions, with a peak in the late night; in constant darkness, they increase, reaching a plateau (8). dCRY resets the clock by interacting with dTIM in the presence of light: subsequent to this interaction, dTIM is phosphorylated and targeted for degradation through a ubiquitin-proteasome mechanism that involves JETLAG, an E3-ubiquitin ligase complex component (9). Upon light activation, dCRY also interacts with JETLAG and is degraded via proteasome (9). dCRY interacts also with the kinase shaggy/GSK3 (SGG), and the cryptochrome's stability in light is considerably increased by this interaction whereas the inactivation of the kinase leads to the degradation of dCRY in darkness (10). The molecular mechanism by which dCRY is activated by light is still not fully understood, but a regulatory role for the C terminus of the protein has been demonstrated by several studies (3, 5, 11–13). The activation of dCRY by light requires a conformational change (13), but the release of a putative repressor cannot be excluded (11). In fact, it has been hypothesized that the activation of dCRY by light is mediated also by specific "regulators" that bind its C terminus, known to regulate the light dependence of dCRY activity (13). This hypothesis was supported by the observation that the C terminus of dCRY is a hotspot for molecular interactions: by in silico analysis and experimental validation, we could identify several protein–protein interaction motifs in this small region and, among them, two class III PDZ-binding motifs (3). PDZ (postsynaptic density protein 95, *Drosophila* disk large tumor suppressor, and zonula occludens-1 protein) domains are modular domains that play a crucial role in the assembly of large protein complexes involved in signaling processes. These domains have a conserved fold consisting of five or six β-strands and two to three α-helices forming a β-stranded sandwich. PDZ domains typically recognize the extreme C terminus of target proteins (14). Distinct PDZ domains bind to optimal sequences, and the structural analysis of known binding sites of PDZ domains and their ligands has provided insight into the specificity of PDZ protein–protein interactions (15). The preference of each residue of a binding peptide is related to the physical-chemical characteristics of different relevant residues on specific secondary structural elements forming the PDZ-binding pocket (16). Three major classes of PDZ-binding motifs have been established (17).

Author contributions: G.M., S.M., R.C., and S.C.E.T. designed research; G.M., A.R., E.L., M.M., C.B., L.C., B.S., A.J.M.M., M.S., R.G., and S.C.E.T. performed research; G.M., C.B., and R.C. analyzed data; and G.M., C.B., C.H.-F., R.C., and S.C.E.T. wrote the paper.

The authors declare no conflict of interest.

This article is a PNAS Direct Submission.

Freely available online through the PNAS open access option.

[1]To whom correspondence should be addressed. E-mail: rodolfo.costa@unipd.it.

This article contains supporting information online at www.pnas.org/lookup/suppl/doi:10.1073/pnas.1212317110/-/DCSupplemental.

NEUROSCIENCE

Here, we show that some functional linear motifs are evolutionarily conserved in the C terminus of cryptochromes, with class III PDZ-binding sites selectively maintained in animals. We detected the presence of dCRY in a multiprotein complex (the Signalplex) involved in the visual-signaling pathway (18), and we found that the interaction with this comlex is mediated by Inactivation No Afterpotential D (INAD), a scaffold protein with five structural PDZ domains. Moreover, we detected a role for dCRY in fly vision.

Results

Functional Motifs Are Conserved in CRY Across Species. We searched for the evolutionary conservation of linear motifs in the C terminus of CRY throughout a broad range of organisms. Linear motifs are short sequences that mediate molecular interactions and very often reside in disordered or nonglobular regions of proteins. Unraveling the evolution of linear motifs is problematic, as these sites tend to be unstable over long evolutionary distances or to jump between different sequence positions inside nonglobular regions. dCRY is an excellent test case for this assumption, as it bears a highly variable C-terminal region that has undergone rapid evolution while maintaining overall similar roles in circadian rhythmicity. An unrooted neighbor-joining phylogenetic tree was constructed using amino acid sequences from various members of the CRY family from plants to humans (Fig. S1). Animal cryptochromes were clustered in four different groups: vertebrate, vertebrate-like (including invertebrate species), CRY4, and *Drosophila*-like. CRY sequences show many linear motifs that are not evenly distributed in all species investigated (Fig. S1). Among them, PDZ domains recognize short sequences at the C terminus of proteins and have an important role in mediating interactions for the assembly of large multiprotein complexes involved in signaling processes at specific subcellular locations. Interestingly, among the three major classes of PDZ-binding motifs, class III is evolutionarily conserved in the CRY C-terminal sequence across animal species (Fig. S1). We speculated that a protein partner of dCRY could be a PDZ domain-containing protein and searched the STRING database (19) for possible candidates. In this database, connections between proteins are based on several methods, including computational predictions. Fig. 1*A* shows the distribution of interactors for dCRY. The results showed a weak connection to No Receptor Potential A (NORPA), a protein belonging to the phototransduction complex (20).

dCRY Interacts with the Phototransduction Complex. In an attempt to identify new partners of dCRY, a coimmunoprecipitation assay, followed by mass spectrometry analysis, was performed on transgenic flies overexpressing a hemagglutinin (HA)-tagged form of dCRY (HACRY; 13) raised in 12:12 light:dark cycles and collected at Zeitgeber Time 24 (ZT24), before lights on, and after a 15-min light pulse. An ~115-kDa species was observed in the sample in the dark and an ~180-kDa species after the light pulse, which were not present in the respective negative controls (Fig. 1*B*). These protein bands were digested in-gel, and the peptide mixtures were analyzed by liquid chromatography–mass spectrometry (LC-MS)/MS using an ESI-QTOF mass spectrometer (21). Analysis of the MS/MS data using the MASCOT software yielded the identification of two proteins involved in the fly visual-signaling pathway: Retinal Degeneration A (RDGA) in the dark and Neither Inactivation Nor Afterpotential C (NINAC) after 15 min of light pulse (Fig. S2*A*) (18, 20). Although RDGA was identified on the basis of the MS/MS spectra of six different tryptic peptides, in the case of NINAC, the identification was based on the MS/MS spectrum of only one peptide displaying a significant score in MASCOT (Fig. S2*B*). The presence of NINACp174 in the complex with HA-tagged form of dCRY (HACRY) was also confirmed by Western blot with an antibody specifically raised against the p174 isoform of the protein that is localized in the rhabdomeres of photoreceptor cells in the

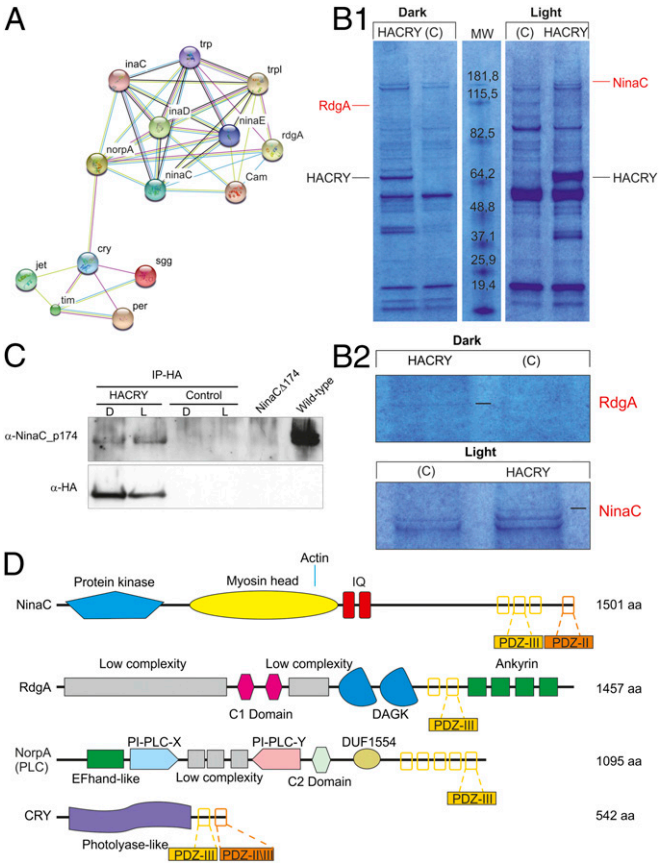

Fig. 1. Interaction of dCRY with the phototransduction complex. (*A*) Protein interaction network surrounding dCRY and INAD. The STRING interaction network is shown for dCRY, INAD, and their main interaction partners with edge colors representing different detection methods. Note that the edge between dCRY and NORPA is based on phenotypic enhancement assays and thus may not necessarily represent a true physical interaction. (*B1*) Coomassie blue-stained gel of heads of protein extracts coimmunoprecipitated with an anti-HA antibody. HACRY-overexpressing flies (HACRY, *yw*;*tim*-GAL4/+; UAS-*HAcry*/+) and relative controls (C, *yw*;*tim*-GAL4) were reared in 12:12 light: dark and collected in the dark (ZT24) and in the light (ZT24 + 15-min light pulse). Molecular masses of markers are indicated (BenchMark Pre-Stained Protein Ladder; Invitrogen). MW, molecular weight. Bands corresponding to HACRY are indicated in black, while stained proteins excised and characterized by mass spectrometry are indicated in red. (*B2*) Zoom of regions of the gel-bearing dRDGA and dNINAC bands. (*C*) Coimmunoprecipitation and Western blot confirming the interaction between HACRY and NINAC in HACRY-overexpressing flies (*yw*;*tim*-GAL4/+; UAS-*HAcry*/+). *tim*-GAL4 flies were used as control. Heads were collected as in *B1*. Membranes were probed with anti-NINACp174 and anti-HA antibodies. *NinaC*$^{\Delta 174}$ and w^{1118} flies, collected at ZT1, were used as negative and positive control, respectively. (*D*) Schematic domain distribution for known and putative INAD interacting proteins. Each protein is drawn proportional to its size, with solid shapes representing different protein domains and their name from the Pfam database. Note that low-complexity regions, shown as light-gray rectangles, are not a proper domain. PDZ-binding motifs are shown as white rectangles with yellow (class III), orange (type II), or peach (overlapping classes II/III) borders.

fly's eye (22). By this procedure, NINACp174 was also detected in the dark, albeit at lower levels than under light conditions (Fig. 1*C*). The difference between NINACp174/HACRY ratios under light and dark conditions was significant ($P < 0.03$, Mann–Whitney U test) (Fig. S2*C*).

dCRY Interacts with the Phototransduction Complex Through INAD. Many of the elements of this visual cascade are assembled in a multiprotein-signaling complex (Signalplex) organized by

INAD, a scaffold protein with five structural PDZ domains, each of which binds to a specific partner (20). A schematic representation of the functional domains of NINAC, RDGA, NORPA, and dCRY is given in Fig. 1*D*. To test whether dCRY interacts with the phototransduction complex through INAD, we searched for INAD in the immunocomplex formed by dCRY. Indeed, a Western blot with an anti-INAD antibody (23), performed on head protein extracts from HACRY-overexpressing flies immunoprecipitated with an anti-HA antibody, revealed that INAD interacts in vivo with dCRY (Fig. 2*A*). The interaction is quite strong in the light, but traces of INAD are visible also in the dark. The difference between INAD/HACRY ratios under light and dark conditions was significant ($P < 0.02$, Mann–Whitney U test) (Fig. S2*D*).

The physical interaction between dCRY and INAD was further analyzed using a yeast two-hybrid system (24), in which a full-length dCRY, directly fused to LexA (bait), was initially challenged with full-length INAD as prey (Fig. 2*B* and Table S1). A strictly light-dependent interaction between the two proteins was observed (Fig. 2*B*, dCRY), which is completely abolished when part of the dCRY C terminus (aa 521–540) is removed. As this region contains the binding motifs for PDZ domains, the 22 C-terminal amino acids of dCRY were tested for the ability to interact with INAD. A light-independent interaction between INAD and the extreme C-terminal tail of dCRY was observed (Fig. 2*B*, dCRY). To examine which domains of INAD are responsible for the interaction with dCRY, prey fusions expressing individual PDZs or different combinations of them were generated and tested for the interaction with full-length dCRY as bait (Fig. 2*B*, INAD). Single PDZ domains did not interact with dCRY, although all of the fusion proteins were correctly expressed in yeast cells. In fact, before the β-galactosidase assay, the expression of all fusion proteins was analyzed by Western blot on yeast lysate with an anti-HA antibody (Fig. S3 and Table S2). For PDZ1, PDZ3, and PDZ4, in addition to the expected signal, a band of molecular weight compatible with a dimeric organization was observed (Fig. S3). However, dimerization of PDZ domains seems not to influence binding to their partners, as the sites involved in the two events are different (25). Because some PDZ domains need other PDZ domains connected in tandem to fold properly and interact with their partners (25), the interaction between dCRY and INAD may also require tandem PDZ domains. However, prey fusions expressing tandems of PDZ linked by their native spacer sequences were still not able to interact with dCRY (Fig. 2*B*, INAD). An in silico analysis performed with CSpritz (26) revealed the presence of an α-helical motif upstream from the PDZ2 domain, specifically the motif MAKI (aa 235–238), which could form a unique extension of the PDZ domain and is also part of the known calmodulin-binding motif. An "extended" version of the PDZ2-PDZ3 tandem prey fusion was generated to include the predicted sites, ranging from residues 207 to 448, and this sequence showed high affinity for dCRY (Fig. 2*B*, INAD). These data suggest that the interaction between INAD and dCRY is mediated by the PDZ2-PDZ3 tandem, but that the PDZ2 domain needs to be extended upstream, with respect to the canonical PDZ domain boundary. Longer fusion sequences were prepared by adding a third PDZ domain; three different portions of INAD, including PDZ1–3 (aa 17–448), PDZ2–4 (aa 249–577), and PDZ3–5 (aa 364–664), respectively, were tested. Only the fusion expressing the N-terminal PDZ1–PDZ3 domains showed affinity for dCRY (Fig. 2*B*, INAD), suggesting that PDZ4 and PDZ5 are not involved in the interaction between dCRY and INAD. The higher binding affinity for the extended PDZ2-PDZ3 tandem compared with larger INAD fragments may be explained by the PDZ2 domain having a non-canonical structure, conferring a higher binding affinity for the dCRY motif. This affinity is likely reduced when PDZ1 is present due to entropy losses caused by increased structural rigidity. The expression levels of all fusions, analyzed by Western blot on yeast lysate with an anti-HA antibody, were comparable (Fig. S3).

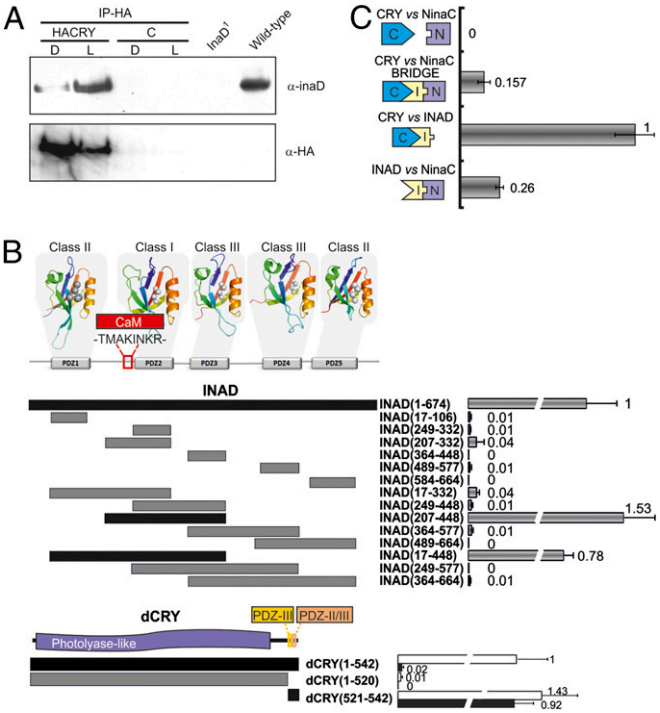

Fig. 2. dCRY interacts with INAD. (*A*) Coimmunoprecipitation and Western blot confirming the interaction between HACRY and INAD in flies overexpressing HACRY (*yw*;*tim*-GAL4/+; UAS-*HAcry*/+). *tim*-GAL4 flies were used as control ("C"). Heads were collected as in Fig. 1*B*. Membranes were probed with anti-INAD and anti-HA antibodies. $inaD^1$ and w^{1118} flies, collected at ZT1, were used as negative and positive controls of the antibody, respectively. (*B*) Identification of the interaction domains of dCRY and INAD using the yeast two-hybrid system. The five INAD PDZ domains are shown where modeled and assigned to putative PDZ subtypes depending on the residue types at the peptide-binding site. Relevant sequence motifs are shown as empty rectangles in the INAD and CRY sequence diagrams. Different domains of INAD were tested for interaction with the full-length dCRY in the presence of light, and different domains of dCRY were tested for interaction with the full-length INAD under both light and dark conditions (open and filled bars, respectively). Interacting fusions are shown in black, and relative β-galactosidase activity (Miller units) is reported for each fusion. Mean ± SEM of at least seven independent clones for each fusion, analyzed in triplicates, is shown. An extended version of the PDZ2–3 tandem, INAD (207–448), exhibits a significantly stronger affinity for dCRY compared with the whole protein ($F_{14,87} = 67.81$, $P < 0.0001$). The interaction between dCRY and INAD occurred in a light-dependent fashion with the C terminus of dCRY being crucial. On the other hand, these last 22 amino acids of the protein showed a light-independent affinity for INAD with a significantly stronger interaction in the light compared with the dark ($t_{13} = 2.6$, $P = 0.02$). (*C*) Yeast two- and three-hybrid assays highlighting that the interaction between dCRY and NINAC is mediated by INAD. The schematic shows the different proteins used as bait or prey fusion: C, dCRY; N, NINAC; I, INAD. Relative β-galactosidase activity (Miller units) is reported for each fusion. Mean ± SEM of at least six independent clones for each fusion, analyzed in triplicates, is shown. The expression of dCRY and NINAC alone does not result in the activation of the reporter gene. The expression of INAD in the yeast nucleus, to generate a three-hybrid system, shows that INAD acts as a structural bridge (BRIDGE) between the two proteins ($F_{3,24} = 57.20$, $P < 0.0001$). The interactions of dCRY–INAD and INAD–NINAC are also shown.

The reported interaction between INAD and NINAC in the formation of the Signalplex (23), together with the interaction between INAD and dCRY that we observed, suggest that the interaction between dCRY and NINAC may be specifically mediated by INAD. To detect whether dCRY, INAD, and NINAC form a ternary protein complex, we devised a three-hybrid system,

in which dCRY was used as bait and NINAC as prey and a FLAG-tagged form of INAD was selectively expressed in the yeast nucleus. The expression of all fusions was tested by Western blot on yeast lysate with anti-HA antibody for NINAC and anti-FLAG antibody for the nuclear INAD (Fig. S3). When we expressed dCRY as bait and NINAC as prey alone, no direct interaction between the two proteins was observed, whereas expression of INAD in the nucleus resulted in the activation of the reporter gene, indicating that the formation of a three-component complex is necessary to restore the activity of the transcription factor (Fig. 2*C*).

dCRY Is Involved in Visual Behavior. The surprising presence of dCRY associated with the visual cascade complex could underline a role, direct or indirect, for this photoreceptor in fly vision, which has not been entertained as yet.

To investigate a possible involvement of dCRY in the fly eye-mediated light response, the electroretinogram (ERG) of flies in which dCRY was completely knocked out (cry^{01}) (27) was analyzed. Moreover, we studied the optomotor and phototactic behavior of cry^{01} flies or flies in which dCRY lacked the C terminus tail (cry^{M}) (5). Wild-type flies are known to show a diurnal rhythm in visual sensitivity determined by ERG recordings, with maximal sensitivity in the first half of the night (28). A comparable rhythm was found in control flies [Canton S (CS) × w^{1118}] with a pronounced sensitivity and a maximum in the middle of the night (Fig. 3*A*). In contrast, the visual sensitivity of cry^{01} mutants was not dependent on the time of day albeit their ERG profiles were normal (Fig. S4*D*). The same was true for the optomotor turning response of the flies. Although the optomotor response of wild-type flies depended significantly on the time of the day (as already observed in ref. 29), it did not in cry^{01} mutants (Fig. 3*B*). cry^{01} mutants responded less to visual stimuli throughout the day than control flies, but this impairment was most evident during the first half of the night, around the wild-type flies' maximum in optomotor turning response (Fig. 3*B*). The optomotor response was analyzed with two different setups (*SI Materials and Methods*) with similar results (Fig. 3 *B* and *C* and Fig. S4 *A* and *B*). Like cry^{01} mutants, cry^{M} mutants also displayed a similar impairment in their optomotor turning response (Fig. S4 *A* and *B*). In a phototaxis assay using countercurrent distribution, in which wild-type flies orient and move toward a light source (30), cry^{01} and cry^{M} mutants showed a reduced performance index of 0.41, compared with 0.63 of the progeny of the CS × w^{1118} cross used as control (Fig. S4*C*). To test whether the impaired optomotor response depends on CRY function in the compound eyes, we selectively rescued CRY in the eyes with the help of the upstream activating sequences (UAS)-GAL4 system, driving GAL4 under control of the eye-specific *glass multiple reporter* (*gmrGAL4*) (31). *gmr-GAL4* is known to disturb the structure of the compound eyes in a dose- and temperature-dependent manner (32). As a consequence, $gmrGAL4;cry^{01}$ control flies showed a lower optomotor response than the other cry^{01} mutants (Fig. 3*C*). Nevertheless, the expression of the $HAcry^{7M}$ construct (Fig. S5) in the compound eyes restored the optomotor response of cry^{01} mutants to almost wild-type levels.

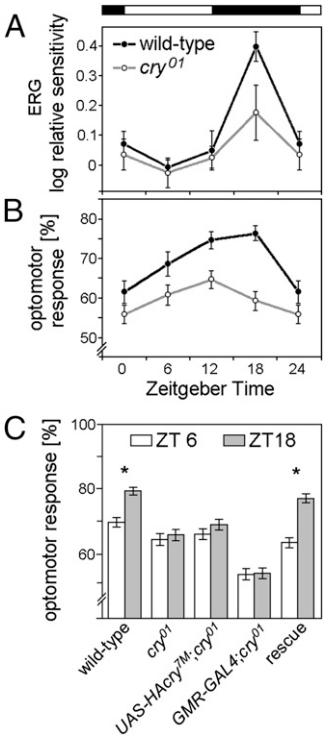

Fig. 3. Visual behavior of wild-type flies, cry^{01} mutants, and cry^{01} mutants with CRY rescue in the eyes. (*A*) Visual sensitivity of cry^{01} and wild-type controls (CS × w^{1118}) during the course of a day. Sensitivity was calculated as the reciprocal of the photon flux needed to evoke a criterion response of 6 mV in the ERG receptor potential. Within each genotype, sensitivity values were normalized to the average sensitivity at ZT6. Each point represents the average of values estimated for a minimum of 9 and a maximum of 13 flies. Mean values ± SEM are given. ANOVA revealed that sensitivity values were significantly dependent on the time of day for CS × w^{1118} ($F_{3,38} = 15.649$, $P < 0.001$) but not for cry^{01} ($F_{3,39} = 1.775$, $P = 0.168$). Note that the value at ZT4 is repeated at ZT0 to improve clarity. (*B*) Optomotor responses of cry^{01} and wild-type controls (CS × w^{1118}) during the course of a day. Each point represents the average of 32 flies. The nonparametric Kruskal–Wallis test revealed that optomotor response values were significantly dependent on the time of day for CS × w^{1118} ($P < 0.001$) but not for cry^{01} ($P = 0.181$). Furthermore, two-way ANOVA showed that optomotor response was highly dependent on the genotype ($F_{1,251} = 31.411$, $P < 0.001$), meaning that wild-type flies generally showed a higher optomotor response than cry^{01} mutants. Note that the value at ZT24 is repeated at ZT0 to improve clarity. (*C*) Optomotor responses at ZT6 and ZT18 for wild-type flies, cry^{01} mutants, and flies with CRY rescued in the compound eyes ($UAS\text{-}HAcry^{7M};cry^{01}$ × $gmrGAL4;cry^{01}$). A total of 100 flies per genotype were analyzed in each experimental condition. Only wild-type and CRY-rescued flies showed a significant difference in optomotor response between the ZT6 and ZT18 (wild type: $t_{198} = 5.23$, $P < 0.0001$; rescued flies: $t_{198} = 6.53$, $P < 0.0001$).

Discussion

The analysis of the linear motifs present in the C terminus of CRYs showed that they were not evenly distributed in all species investigated. The class III PDZ motif is present in all animal phyla, suggesting a functional constraint on the evolving sequence, as the motif is maintained although it is not being conserved in the same sequence stretch. Our results clearly indicate that the circadian blue-light photoreceptor dCRY interacts with the visual transduction complex (Signalplex) through the scaffold protein INAD. The interaction between the two proteins is mediated by a specific region of INAD, which includes the PDZ2-PDZ3 tandem, but is extended upstream with respect to the canonical PDZ domain boundary to include a stretch of amino acids known to be part of a calmodulin-binding motif. Interactions modulated by multiple INAD PDZ domains have already been described (33). It has also been reported for other PDZ-containing proteins that two or three PDZ domains connected in tandem may exhibit different specificity in their target-binding properties compared with isolated domains (34). We also established that the 22-amino acid C-terminal sequence of dCRY is involved in binding to INAD, in accordance with the presence of either class III or class II/III PDZ-binding motifs predicted by the eukaryotic linear motif (ELM) program in the C terminus of the protein and also with the notion that PDZ domains preferentially interact with the absolute carboxyl-terminal

ends of their target proteins (14). The interaction between dCRY and INAD is particularly effective in the light, and it is well recognized that the activity of both proteins is modulated by light. However, the light-independent interaction of the C-terminal fragment of dCRY with INAD suggests that the influence of light in the interaction of the full-length proteins is due to the PHR domain of dCRY. Supporting this hypothesis is the fact that the INAD PDZ4 and -5, known to be regulated by light-dependent conformational changes (33), are not involved in the interaction. The interaction between dCRY and NINAC observed in vivo represents quite an unexpected result. A connection between dCRY and a cardinal component of the fly visual cascade (23) was established, and the mediator role of INAD in the interaction was demonstrated. We also showed that this interaction has a functional importance for vision. In CRY-knockout flies, the diurnal cycling of photoreceptor sensitivity and motion vision typical of wild-type flies (28, 29) is abolished. Furthermore, the CRY-knockout flies are slightly but significantly impaired in motion vision. The diurnal rhythm in optomotor response was recovered when CRY was expressed in all photoreceptor cells of the compound eyes, showing that CRY in the photoreceptor cells is responsible for wild-type rhythms in motion vision. Motion detection depends mainly on intact vision in photoreceptors R1–6 with minor contribution from R7 and R8 (35, 36), whereas phototaxis is mediated by all eight photoreceptors in the compound eyes (37). dCRY is expressed in the entire cytoplasm of the photoreceptor cells and seems to have the highest density close to the rhabdomers, the place of the visual cascade (38). Therefore, dCRY may easily interact with INAD and eventually modulate the transient receptor potential (TRP) and TRP-like (TRPL) channel opening in interplay with the other PDZ proteins of the Signalplex. Interestingly, small amounts of CRY seem to be sufficient for this interaction as the optomotor response was highest at the end of the day until the middle of the night (ZT12–18) when CRY levels are low (9). Recently, dCRY was shown to be also involved in the membrane excitability (K^+ channel conductance) of the large ventral Lateral clock Neurons (l-LN_v) (39). These neurons fire action potential upon illumination with blue light, and this firing is dependent on dCRY. Although the way in which dCRY regulates the l-LN_v firing rate in relation to K^+ channel conductance remains unclear, our results further support an involvement of dCRY in membrane potential modulation. Here, we show that dCRY may be the link that couples the clock with the PDZ proteins of the Signalplex, in this way modulating vision in a circadian fashion. A functional circadian clock in the photoreceptor cells is obviously important to control visual coding efficiency in *Drosophila* and to optimize vision under different light intensity regimes (29). In fact, wild-type flies show circadian changes in the size of certain brain regions (e.g., optic lobes) and in photoreceptor cell terminals that control the sensitivity of photoreceptors to circadian variations in light levels (29). This structural plasticity is still maintained in period $(per)^{01}$ flies, which lack a key component of the circadian machinery, but it is exclusively light-driven as there is no longer "anticipation" of the light/dark transitions (29). In most invertebrates, the components of visual signaling are localized on the rhabdomeres (40), whereas a ciliary vision (rods and cones) is predominant in the vertebrate retina (41). An important difference between the two kinds of photoreceptors is the biochemical cascade used to transduce photic signals in electric signals. In fact, rods and cones use a cascade involving cyclic guanyl monophosphate as a second messenger whereas rhabdomeric photoreceptors use a phosphoinositide-signaling cascade involving the enzyme phospholipase C (PLC) (41). Retinal photoreception in mammals includes a subset of retinal ganglion cells that are able to respond to light even in the absence of synaptic inputs (42). These cells, called "intrinsically photosensitive retinal ganglion cells" (ipRGCs), use melanopsin as photopigment and send their axons directly to the suprachiasmatic nucleus, the site of the primary circadian pacemaker in mammals (18, 41). ipGRCs have been shown to use a rhabdomeric-like phosphoinositide cascade involving the effector enzyme PLC (18, 41). Very recently, it has been observed that these melanopsin-expressing ganglion cells extend their projections toward the thalamo-cortical neurons implicated in pattern vision, establishing melanopsin-based photoreception as a significant source of visual information to the thalamo-cortical pathway, independent of rods or cones (43). The ipGRCs and the fly phototransduction mechanisms also share other similarities: both require a member of the Gq/11 family of G proteins as a mediator of the phototransduction cascade, and, in both cases, the phototransduction cascade is tightly coupled to the plasma membrane and involves light-sensitive channels belonging to the TRP family (44). The similarity of the photoreception cascade between *Drosophila* and the mammalian ipRGCs, and also the expression of CRY in both photoreceptor cells (45), raises the question of whether mammalian CRYs could contribute to the circadian functions of ipRGCs by specifically binding to the phototransduction complex. Although a homologous complex of the fly Signalplex has not been described in ipRGCs, several components of this multiprotein complex seem to be conserved (18). Specifically, a protein homolog of dINAD, INAD-like (INADL), bearing seven PDZ domains, has been identified in humans (46). A search for a functional protein interaction network, performed with the STRING database (Fig. S6), showed that INADL can be a functional partner of Crumbs homolog 1 precursor, a factor involved in retinal photoreceptor organization (47). This renders INADL a good candidate for a scaffold protein that organizes and maintains the phototransduction complex in ipRGCs. Our results extend the role of dCRY to fly visual biology and provide a tantalizing glimpse of a phylogenetically conserved possible role for CRY that may have circadian implications in mammalian vision also.

Materials and Methods

Bioinformatic Analyses. The computational search for dCRY protein–protein interactions combined the results from the STRING database (19) of protein–protein interactions with the domain organization of proteins from Pfam (48). Relevant proteins were analyzed with CSpritz (26), which predicts intrinsic disorder in the sequence as well as linear motifs coding for common protein–peptide interactions taken from ELM (49). The X-ray structures of INAD PDZ domains were retrieved from the Protein Data Bank for domains 1 and 5 [Protein Data Bank (PDB) codes 1IHJ and 2QKT]. The three remaining domains were identified (50) and modeled based on PDB codes 2FNE (chain C) and 1Z87 (chain A) as templates for PDZ2-PDZ4 and PDZ3, respectively (Fig. S7).

Coimmunoprecipitation and Mass Spectrometry. Head extracts from HACRY-overexpressing flies were subjected to coimmunoprecipitation as previously described (3). After the separation of proteins by SDS/PAGE, Coomassie-stained protein bands were excised, in-gel digested (21), and analyzed by LC-MS/MS on a Micromass CapLC unit (Waters) interfaced to a Micromass Q-Tof Micro mass spectrometer (Waters). MS/MS data were analyzed by MASCOT software (Matrix Science; www.matrixscience.com/) against the *Drosophila* sequences of the Swiss-Prot database (release 2011_03).

Western Blots. Immunocomplexes were analyzed by Western blotting using the following antibodies: rabbit polyclonal anti-INAD (1:500) (25), rabbit polyclonal anti-NINACp174 (1:500) (22), and mouse anti-HA (Sigma; 1:5,000).

Yeast Two- and Three-Hybrid Tests. dCRY, either full-length or fragments, was fused to the LexA moiety in the bait vector (pEG202), and INAD (full length or fragments) was fused to the "acid-blob" portion of the prey vector (pJG4-5) (24). In the yeast three-hybrid assay, dCRY was used as bait and NINAC as prey, and a FLAG-tagged full-length INAD was expressed in the nucleus. Quantification of β-galactosidase activity was performed in liquid culture as in Ausbel et al. (51).

Visual Sensitivity Determined by ERG Recordings. Visual sensitivity was obtained from the irradiance response curves (IRC) recorded at four different ZTs. The ERG responses to light stimuli of different intensities were used to determine the IRCs. ERGs were recorded as in ref. 28.

Analysis of Optomotor Activity. The walking optomotor test was performed as in ref. 52 (setup 1 in *SI Materials and Methods*). Details of setups 1 and 2 are given in *SI Materials and Methods*.

Phototaxis. The experiments for phototaxis were performed as described in ref. 30. See details in *SI Materials and Methods*.

ACKNOWLEDGMENTS. We thank Michele Vidotto (University of Padova) for help with the initial linear motif analysis; Paola Cisotto (University of Padova) for technical support; Matteo Simonetti (University of Padova) for graphical support; Alberto Biscontin (University of Padova) for help with quantitative RT-PCR; Craig Montell (The Johns Hopkins University School of Medicine) for anti-INAD and anti-NINACp174 antibodies; Dr. Susan Tsunoda (Colorado State University) for $inaD^{1}$ flies; the Bloomington Stock Center for $NinaC^{\Delta 174}$ flies; and Dr. Taishi Yoshii (Okayama University) for $gmrGAL4;cry^{01}$ flies. We thank Reinhard Wolf (Virchow Center, University of Würzburg) for help with the optomotor response experiments and Reinhard Wolf and Bambos Kyriacou (University of Leicester) for helpful comments on the manuscript. This work was funded by grants from the European Community (Sixth Framework Project Entrainment of the Circadian Clock 018741) and Fondazione Cariparo (Progetti di Eccellenza 2011–2012) (R.C.); University of Padova Grant CPDA099390/09 (to G.M.); and University of Padova Grants CPDA098382 and CPDR097328 and Fondo Investimento Ricerca di Base (FIRB) Futuro in Ricerca Grant RBFR08ZSXY (to S.C.E.T.). R.C. was supported by the Italian Space Agency [Disturbo del Controllo Motorio e Cardiorespiratorio (DCMC) grant] and the Ministero dell'Università e della Ricerca. C.H.-F. was supported by the Deutsche Forschungsgemeinschaft (Fo207/10-3), R.G. by the Graduate School of Life Sciences (University of Würzburg), and M.S. by the Hanns Seidel Foundation.

1. Hardin PE (2011) Molecular genetic analysis of circadian timekeeping in *Drosophila*. *Adv Genet* 74:141–173.
2. Chaves I, et al. (2011) The cryptochromes: Blue light photoreceptors in plants and animals. *Annu Rev Plant Biol* 62:335–364.
3. Hemsley MJ, et al. (2007) Linear motifs in the C-terminus of *D. melanogaster* cryptochrome. *Biochem Biophys Res Commun* 355(2):531–537.
4. Lin C, Todo T (2005) The cryptochromes. *Genome Biol* 6(5):220.
5. Busza A, Emery-Le M, Rosbash M, Emery P (2004) Roles of the two *Drosophila* CRYPTOCHROME structural domains in circadian photoreception. *Science* 304(5676): 1503–1506.
6. Yuan Q, Metterville D, Briscoe AD, Reppert SM (2007) Insect cryptochromes: Gene duplication and loss define diverse ways to construct insect circadian clocks. *Mol Biol Evol* 24(4):948–955.
7. Gegear RJ, Foley LE, Casselman A, Reppert SM (2010) Animal cryptochromes mediate magnetoreception by an unconventional photochemical mechanism. *Nature* 463(7282):804–807.
8. Emery P, So WV, Kaneko M, Hall JC, Rosbash M (1998) CRY, a *Drosophila* clock and light-regulated cryptochrome, is a major contributor to circadian rhythm resetting and photosensitivity. *Cell* 95(5):669–679.
9. Peschel N, Chen KF, Szabo G, Stanewsky R (2009) Light-dependent interactions between the Drosophila circadian clock factors cryptochrome, jetlag, and timeless. *Curr Biol* 19(3):241–247.
10. Stoleru D, et al. (2007) The Drosophila circadian network is a seasonal timer. *Cell* 129(1):207–219.
11. Rosato E, et al. (2001) Light-dependent interaction between Drosophila CRY and the clock protein PER mediated by the carboxy terminus of CRY. *Curr Biol* 11(12):909–917.
12. Dissel S, et al. (2004) A constitutively active cryptochrome in *Drosophila melanogaster*. *Nat Neurosci* 7(8):834–840.
13. Ozturk N, Selby CP, Annayev Y, Zhong D, Sancar A (2011) Reaction mechanism of Drosophila cryptochrome. *Proc Natl Acad Sci USA* 108(2):516–521.
14. Saras J, Heldin CH (1996) PDZ domains bind carboxy-terminal sequences of target proteins. *Trends Biochem Sci* 21(12):455–458.
15. Songyang Z, et al. (1997) Recognition of unique carboxyl-terminal motifs by distinct PDZ domains. *Science* 275(5296):73–77.
16. Chen JR, Chang BH, Allen JE, Stiffler MA, MacBeath G (2008) Predicting PDZ domain-peptide interactions from primary sequences. *Nat Biotechnol* 26(9):1041–1045.
17. Tonikian R, et al. (2008) A specificity map for the PDZ domain family. *PLoS Biol* 6(9):e239.
18. Montell C (2012) Drosophila visual transduction. *Trends Neurosci* 35(6):356–363.
19. Szklarczyk D, et al. (2011) The STRING database in 2011: Functional interaction networks of proteins, globally integrated and scored. *Nucleic Acids Res* 39(Database issue):D561–D568.
20. Wang T, Montell C (2007) Phototransduction and retinal degeneration in *Drosophila*. *Pflugers Arch* 454(5):821–847.
21. Wilm M, et al. (1996) Femtomole sequencing of proteins from polyacrylamide gels by nano-electrospray mass spectrometry. *Nature* 379(6564):466–469.
22. Porter JA, Hicks JL, Williams DS, Montell C (1992) Differential localizations of and requirements for the two Drosophila ninaC kinase/myosins in photoreceptor cells. *J Cell Biol* 116(3):683–693.
23. Wes PD, et al. (1999) Termination of phototransduction requires binding of the NINAC myosin III and the PDZ protein INAD. *Nat Neurosci* 2(5):447–453.
24. Golemis EA, Brent R (1997) *Searching for Interacting Proteins with the Two-Hybrid System III. In the Yeast Two-Hybrid System*, eds Bartel PL, Field S (Oxford University Press, New York), pp 43–72.
25. Feng W, Shi Y, Li M, Zhang M (2003) Tandem PDZ repeats in glutamate receptor-interacting proteins have a novel mode of PDZ domain-mediated target binding. *Nat Struct Biol* 10(11):972–978.
26. Walsh I, et al. (2011) CSpritz: Accurate prediction of protein disorder segments with annotation for homology, secondary structure and linear motifs. *Nucleic Acids Res* 39(Web Server issue):W190–W196.
27. Dolezelova E, Dolezel D, Hall JC (2007) Rhythm defects caused by newly engineered null mutations in Drosophila's cryptochrome gene. *Genetics* 177(1):329–345.
28. Chen DM, Christianson JS, Sapp RJ, Stark WS (1992) Visual receptor cycle in normal and *period* mutant *Drosophila*: Microspectrophotometry, electrophysiology, and ultrastructural morphometry. *Vis Neurosci* 9(2):125–135.
29. Barth M, Schultze M, Schuster CM, Strauss R (2010) Circadian plasticity in photoreceptor cells controls visual coding efficiency in *Drosophila melanogaster*. *PLoS ONE* 5(2):e9217.
30. Benzer S (1967) Behavioral mutants of *Drosophila* isolated by countercurrent distribution. *Proc Natl Acad Sci USA* 58(3):1112–1119.
31. Freeman M (1996) Reiterative use of the EGF receptor triggers differentiation of all cell types in the *Drosophila* eye. *Cell* 87(4):651–660.
32. Kramer JM, Staveley BE (2003) GAL4 causes developmental defects and apoptosis when expressed in the developing eye of *Drosophila melanogaster*. *Genet Mol Res* 2(1):43–47.
33. Liu W, et al. (2011) The INAD scaffold is a dynamic, redox-regulated modulator of signaling in the *Drosophila* eye. *Cell* 145(7):1088–1101.
34. Long JF, et al. (2003) Supramodular structure and synergistic target binding of the N-terminal tandem PDZ domains of PSD-95. *J Mol Biol* 327(1):203–214.
35. Yamaguchi S, Wolf R, Desplan C, Heisenberg M (2008) Motion vision is independent of color in *Drosophila*. *Proc Natl Acad Sci USA* 105(12):4910–4915.
36. Wardill TJ, et al. (2012) Multiple spectral inputs improve motion discrimination in the Drosophila visual system. *Science* 336(6083):925–931.
37. Yamaguchi S, Heisenberg M (2011) Photoreceptors and neural circuitry underlying phototaxis in insects. *Fly (Austin)* 5(4):333–336.
38. Yoshii T, Todo T, Wülbeck C, Stanewsky R, Helfrich-Förster C (2008) Cryptochrome is present in the compound eyes and a subset of Drosophila's clock neurons. *J Comp Neurol* 508(6):952–966.
39. Fogle KJ, Parson KG, Dahm NA, Holmes TC (2011) CRYPTOCHROME is a blue-light sensor that regulates neuronal firing rate. *Science* 331(6023):1409–1413.
40. Shieh BH, Niemeyer B (1995) A novel protein encoded by the InaD gene regulates recovery of visual transduction in *Drosophila*. *Neuron* 14(1):201–210.
41. Graham D (2008) Melanopsin ganglion cells: A bit of fly in the mammalian eye. *Webvision: The Organization of the Retina and Visual System*, eds Kolb H, Fernandez E, Nelson R (University of Utah, Health Sciences Center, Salt Lake City). Available at http://webvision.med.utah.edu/book/part-ii-anatomy-and-physiology-of-the-retina/elanopsin-ganglion-cells-a-bit-of-fly-in-the-mammalian-eye.
42. Bailes HJ, Lucas RJ (2010) Melanopsin and inner retinal photoreception. *Cell Mol Life Sci* 67(1):99–111.
43. Brown TM, et al. (2010) Melanopsin contributions to irradiance coding in the thalamo-cortical visual system. *PLoS Biol* 8(12):e1000558.
44. Graham DM, et al. (2008) Melanopsin ganglion cells use a membrane-associated rhabdomeric phototransduction cascade. *J Neurophysiol* 99(5):2522–2532.
45. Thompson CL, et al. (2003) Expression of the blue-light receptor cryptochrome in the human retina. *Invest Ophthalmol Vis Sci* 44(10):4515–4521.
46. Vaccaro P, et al. (2001) Distinct binding specificity of the multiple PDZ domains of INADL, a human protein with homology to INAD from *Drosophila melanogaster*. *J Biol Chem* 276(45):42122–42130.
47. den Hollander AI, et al. (2002) Isolation of Crb1, a mouse homologue of Drosophila crumbs, and analysis of its expression pattern in eye and brain. *Mech Dev* 110(1–2): 203–207.
48. Finn RD, et al. (2010) The Pfam protein families database. *Nucleic Acids Res* 38(Database issue):D211–D222.
49. Gould CM, et al. (2010) ELM: The status of the eukaryotic linear motif resource. *Nucleic Acids Res* 38(Database issue):D167–D180.
50. Bindewald E, Cestaro A, Hesser J, Heiler M, Tosatto SC (2003) MANIFOLD: Protein fold recognition based on secondary structure, sequence similarity and enzyme classification. *Protein Eng* 16(11):785–789.
51. Ausbel FM, et al. (1989) *Current Protocols in Molecular Biology* (Green Publishing Associated, New York).
52. Zordan MA, et al. (2006) Post-transcriptional silencing and functional characterization of the Drosophila melanogaster homolog of human Surf1. *Genetics* 172(1): 229–241.

Supporting Information

Mazzotta et al. 10.1073/pnas.1212317110

SI Text

We supposed that the interaction between *Drosophila* CRYPTOCHROME (dCRY) and Inactivation No Afterpotential D (INAD) occurs through the conserved class III PDZ-binding motif in the C-terminal tail of dCRY and one or more of the five PDZ domains of INAD. To identify the possible PDZ domain responsible for the interaction, we investigated the binding specificity of each domain. Because the binding preference of any PDZ domain is significantly determined by the chemical characteristic of the αB1 residue of the binding pocket and the p(−2) residue of the ligand motif, we collected structural and sequence information about PDZ domains and ligands of INAD. For two of the five PDZ domains, PDZ1 and PDZ5, a crystal structure had been previously solved (1, 2) whereas for the other three PDZ domains (PDZ2, PDZ3, and PDZ4) we built a model using a homology modeling approach. To identify relevant positions on the peptide-binding pocket of each domain, we built a structural alignment of the five domains. As described in Fig. S7, each domain has the highly conserved carboxylate-binding loop (X-Φ-G-Φ motif, where X is any amino acids and Φ is a hydrophobic residue) between βA and βB strands. Furthermore, the chemical characteristics of the distinct residues at position αB1 suggest a possible binding preference for each PDZ domain (3). On the basis of these speculations, PDZ1 could be classified in the IIB subclass where the negative or polar residue at αB1 has been associated with tyrosine (Tyr) or phenylalanine (Phe) at the p(−2) position in the ligand motif (3). However, PDZ1 was crystallized with the C terminus peptide of No Receptor Potential A (NORPA) phospholipase C (PLC)-β, revealing a unique mode of interaction that consists of a disulfide bond between cysteine 31 (Cys31) of PDZ1 and Cys(p-1) of the NORPA peptide (1). Furthermore, the C-terminal sequences of NORPA (PLC-β) and Neither Inactivation Nor Afterpotential C (NINAC) (-EFCA; -AVDI; respectively), another previously identified partner of INAD (4), matched well with the class II PDZ domain-binding motif Φ-X-Φ-COO-. The other domain of INAD that could be assigned to this class is the PDZ5 domain, which has an aromatic residue (Phe) at the αB1 position. PDZ5 was also found to interact with NORPA (PLC-β) (5), and the interaction seems to occur through the C-terminal class II PDZ-binding motif or through an internal region of NORPA (6). Different groups proposed that the INAD–NORPA interaction occurs either with both PDZ1 and PDZ5 domains (7) or with PDZ5 only (5). The lack of interaction with NORPA (PLC-β) reported by other groups (2, 8) was probably due to interference of the experimental conditions used (e.g., posttranslational modification) as PDZ5 is phosphorylated by PKC (8, 9) and undergoes a redox conformational switch that dramatically reorganizes the binding pocket (2, 10). The PDZ2 domain, with a His residue at the αB1 position, was assigned to class I PDZ interactions. These PDZ domains recognize ligands that contain either serine or threonine (Thr) at the −2 postion. The PDZ2 of INAD was found to recognize the unique class I PDZ-binding motifs predicted by the eukaryotic linear motif (ELM) program at the C-terminal sequence of eye-PKC (-ITII) (11). The class III PDZ-binding motifs instead could be preferential ligands for PDZ3 and PDZ4 domains, which have Tyr and Thr, respectively, at the αB1 position. The hydroxyl group of these residues can bind a negatively charged amino acid in the p(−2) position of the ligand motif. PDZ3 was identified as a target PDZ domain for the TRP calcium channel (5, 12) and PDZ4 as a target for eye-PKC (5). It has been demonstrated (8) that either PDZ3L (extra 28 residues COOH-terminal to PDZ3) or PDZ4 was sufficient to bind opsin, TRPL, and PKC. In this work, Xu et al. (8) demonstrated that the binding with PKC could occur through a binding site in the C terminus different from those at the extreme C terminus interacting with PDZ2. Furthermore, PDZ3 and PDZ4 domains, using a different interface, also mediate the INAD homo-multimerization (8). Little is known about the ligand motifs mediating interactions with domains PDZ3 and PDZ4, but all of the detected interacting proteins contain several class III PDZ-binding motifs predicted by the ELM program in the internal sequence of their C terminus (Fig. 1*D*).

SI Materials and Methods

In Silico Protein–Protein Interactions. The computational search for protein–protein interactions was started by using the annotated STRING database (13) of known and predicted physical and functional protein–protein interactions. Using STRING in protein mode, we obtained the protein interaction network of dCRY (Fig. 1*A*) and selected interactions with high confidence levels. To explore the domain organization of proteins (Fig. 1*D*), identified by SMART (14) and predicted or found to be related to CRY, we used the interactive view of the STRING network. The CRY C termini were analyzed using CSpritz (15), which predicts intrinsic disorder in the sequence as well as secondary structure preferences. Linear motifs coding for common protein–peptide interactions, taken from ELM (16), are also predicted in CSpritz.

Phylogenetic Tree Reconstruction. A multiple sequence alignment with 98 sequences from Photolyase/Cryptochrome families available in UniProt database (www.uniprot.org) was generated with ClustalW2 (17). Sequences are representative of either different cryptochrome families or different animal/plant phyla. Alignments were manually verified and a phylogenetic tree was generated using neighbor-joining methods (18) with a complete deletion mode (Fig. S1). A total of 1,196 sites (953 variable and 52 conserved sites), including gap sites, were used in the phylogenetic analysis. Bootstrap tests were performed with 1,000 replications. PAM matrix correction distance was adopted, and rates among sites were set as uniform. This analysis was performed in April 2011.

In Silico Analysis of INAD. Domain organization was defined by data retrieved from the Pfam resource (19). Secondary structure was predicted using a consensus method (20), and disordered regions were searched for with CSpritz (15). The crystal structure of INAD PDZ1/PDZ5 domains was retrieved from the Protein Data Bank (PDB) database (21) (PDB codes 1IHJ and 2QKT). Models for the other three INAD-PDZ domains (Fig. 2*B*) were constructed using the HOMER server (http://protein.bio.unipd.it/homer/). The automatic template search with MANIFOLD (22) indicated 2FNE (chain C) and 1Z87 (chain A) as templates for PDZ2/PDZ4 and PDZ3, respectively. The raw models generated from these templates were completed by modeling the divergent regions with LOBO, a fast divide-and-conquer method (23). The final models were subjected to a short steepest-descent energy minimization with GROMACS (24) and evaluated with QMEAN (25, 26). The structure was visualized using PyMOL (DeLano Scientific; http://pymol.sourceforge.net/). To predict potential functional motifs, protein sequences were analyzed using ELM (16).

Fly Strains. The following *Drosophila* strains were used: w^{1118}; *Oregon-R*; WT-ALA (27); the progeny of crosses *Canton S* × w^{1118} and WT-ALA × w^{1118} as wild-type controls; $inaD^{1}$ (28); $NinaC^{\Delta 174}$ (29); cry^{0} (30); cry^{M} (31); *yw; timGal4* (32); *w; UAS-HAcry* 16.1 (33), and $UAS\text{-}HAcry^{7M};cry^{0}$, $gmrGal4;cry^{0}$. All flies were reared on a standard yeast–glucose–agar medium and maintained at 23 °C, 70% relative humidity, on a 12-h light:12-h dark cycle.

Coimmunoprecipitation. Three- to five-day-old flies overexpressing HA-dCRY (*yw*; *tim-GAL4/+; UAS-HAcry/+*) were collected at Zeitbeger time 24 (ZT24) (ZT0 lights-on and ZT12 lights-off in a 12:12 light–dark cycle) and after a 15-min light pulse given at the same time point. Heads were homogenized in extraction buffer [20 mM Hepes, pH 7.5, 100 mM KCl, 2.5 mM EDTA, pH 8, 5% glycerol, 0.5% (vol/vol) Triton X-100, 1 mM DTT, complete protease inhibitors (Roche)] and centrifuged at maximum speed for 10 min, and the supernatant was precleared with protein-G agarose beads (Sigma) for 20 min. The extract was then incubated with anti-HA (1:1,000; Sigma) for 2 h at 4 °C before the addition of 30 μL of protein G agarose beads (1:1 slurry) for 1 h. The beads were precipitated by centrifugation at 2,000 × *g* and then washed three times with 1 mL of extraction buffer and once with 1 mL of 20 mM Hepes, pH 7.5.

For electrophoresis, proteins were detached from the beads by the addition of NuPAGE LDS sample buffer (Invitrogen) and heating at 70 °C for 10 min and analyzed by SDS/PAGE on 4–12% (wt/vol) NuPAGE Novex Bis-Tris Gels (Invitrogen).

Protein Identification by Mass Spectrometry. After the separation of proteins by SDS/PAGE, Coomassie-stained protein bands were excised and digested in-gel (34). Briefly, gel pieces were destained, and the proteins were reduced with DTT, alkylated with iodoacetamide, and digested with porcine trypsin (modified sequencing grade; Promega) overnight at 37 °C. The supernatants were then transferred to other tubes, and residual tryptic peptides were extracted upon incubation of gel spots with 25 mM NH_4HCO_3 at 37 °C for 15 min, followed by shrinking of gel pieces with acetonitrile and incubation with 5% (vol/vol) formic acid at 37 °C for 15 min, followed by shrinking with acetonitrile. The extracts were combined with the primary supernatant and dried in a SpeedVac centrifuge (Savant Instruments Inc.). Protein digests were then resuspended in 0.1% (vol/vol) trifluoroacetic acid and 5% (vol/vol) acetonitrile and analyzed by liquid chromatography–mass spectrometry (LC-MS)/MS. LC-MS/MS analyses were performed on a Micromass CapLC unit (Waters) interfaced to a Micromass Q-Tof Micro mass spectrometer (Waters) equipped with a nanospray source. Tryptic digests were loaded at a flow rate of 20 μL/min onto an Atlantis dC18 Trap Column. After valve switching, the sample was separated on a Symmetry C_{18} column (150 × 0.075 mm, 3.5-μm particle size) (Waters) at a flow rate of 3.8 μL/min using a gradient from 5 to 15% (vol/vol) B in 3 min and from 15 to 50% (vol/vol) B in 22 min [solvent A: 95% (vol/vol) H_2O, 5% (vol/vol) acetonitrile, 0.1% (vol/vol) formic acid; solvent B: 5% (vol/vol) H_2O, 95% (vol/vol) acetonitrile, 0.1% (vol/vol) formic acid]. Instrument control and data acquisition and processing were achieved with MassLynx V4.1 software (Waters). MS/MS data were analyzed by MASCOT software (Matrix Science; www.matrixscience.com/) against the *Drosophila* sequences of the Swiss-Prot database (release 2011_03). The following parameters were used in the MASCOT search: trypsin specificity; maximum number of missed cleavages—3; fixed modification—carbamidomethyl (Cys); variable modifications—oxidation (Met); peptide mass tolerance—± 0.5 Da; fragment mass tolerance—± 0.5 Da; protein mass—unrestricted; mass values— monoisotopic.

Western Blot. Following transfer onto nitrocellulose filters, proteins were analyzed by Western blotting using the following antibodies: rabbit polyclonal anti-INAD (4; 1:500), rabbit polyclonal anti-NINACp174 (29; 1:500), mouse anti-HA (Sigma; 1:5,000), and mouse anti-FLAG (1:5,000). For quantification of the immunodetected signals, each film was analyzed with Image J software (available at http://rsb.info.nih.gov/ij; developed by Wayne Rasband, National Institutes of Health). Relative abundance of NINAC and INAD were defined as a ratio with HA-tagged form of dCRY (HACRY) (NINAC/HACRY and INAD/HACRY, respectively).

Yeast Two-Hybrid Assays. All of the experiments were performed in the EGY48 yeast strain (MATα, *ura3*, *trp1*, *his3*, 3*Lex*A-operator-*LEU*), and dCRY, either full length or in fragments, was fused to the LexA moiety in the bait vector (pEG202); INAD (full length or in fragments) was fused to the "acid-blob" portion of the prey vector (pJG4-5) (35). The full-length INAD-coding sequence was amplified from cDNA extracted from heads of w^{1118} flies with primers INAD-FL-F (Table S1), which add NdeI-EcoRI-AatII restriction sites, and INAD-FL-R (Table S1), which add XbaI, XhoI, and HinIII restriction sites, by using the Phusion High-Fidelity DNA Polymerase (New England Biolabs). The PCR product was digested with EcoRI and XhoI and directionally cloned in the pJG4-5 vector. All of the constructs with the different INAD fragments were obtained with the same strategy—by using pJG-INAD full length as template. The primers used are listed in Table S1; the reverse primers incorporate a TAG stop codon before the XbaI restriction site. All of the constructs were fully sequenced to assess the in-frame insertion of the cDNA and to control for unwanted mutations. The reliable expression of prey fusions in the EGY48 yeast strain (MATα, *ura3*, *trp1*, *his3*, 3*Lex*A-operator-*LEU*) transformed with the bait vector and *LacZ* reporter plasmid pSH18-34 was confirmed by immunoblot. Protein extracts were obtained as in ref. 36, subjected to SDS/PAGE (NuPAGE-Invitrogen), and probed with a specific anti-HA antibody (Sigma; 1:5,000). Expected molecular weights for the tested fusions are listed in Table S3. Quantification of β-galactosidase activity was performed in liquid culture as in ref. 36, and each experiment was repeated at least three times.

Yeast Three-Hybrid Assay. In this experiment, dCRY full-length was used as bait and NINACp174 as prey. The coding sequence of NINACp174 was amplified from cDNA extracted from heads of w^{1118} flies with primers NINAC-5F and NINAC-PBR (Table S1) that add a SalI site at both ends. The PCR product was digested with SalI and cloned in the pJG4-5 vector linearized with XhoI. Clones with the insert in the right orientation were fully sequenced to assess the in-frame insertion of the cDNA and to control for unwanted mutations. The expression of NINAC was assessed by Western blot with the anti-HA antibody. The expression of INAD in the yeast nucleus was achieved by cloning the full-length cDNA in pLEU, a modified version of the pDBLeu vector (Invitrogen), where the DNA-binding domain was removed by restriction with HindIII and SalI. The coding sequence of INAD was amplified with primers inaD-NLS-FLAG_F that add an HindIII site at the 5′ end, in-frame with sequences for a nuclear localization signal and a FLAG tag, and inaD-Xho-R that adds an XhoI site at the 3′ end. The PCR fragment was digested with HindIII and XhoI and directionally cloned in pLEU HindIII-SalI. Positive clones were sequenced to check for unwanted mutations. The expression of the nuclear form of INAD was assessed by Western blot on protein extracts with a specific anti-FLAG antibody (Sigma; 1:500). β-Galactosidase activity was quantified as previously described.

Visual Sensitivity (Electroretinograms). ***Preparation and Recording.*** Male flies at the age of 6–8 d, between ZT6 and ZT24, were slightly anesthetized with carbon dioxide and fixed with their ventral side to a small acrylic glass plate using dental wax (ESPE

Protemp II). Legs, wings, proboscis, and heads were also fixed to the plate without impairing the respiratory movement of the fly. The preparation was then transferred to the stage of a stereo microscope. A chloridized silver wire (D = 0.38 mm) that served as the reference electrode was inserted into the thorax of the fly. The recording electrode, a glass microelectrode pulled from borosilicate capillaries (i.d. = 0.58 mm, OD = 1.00 mm, L = 80 mm with filament) with a DMZ puller (Zeitz Instruments) and filled with Insect Ringer, was placed on the surface of the compound eye. The stereo microscope as well as the reference and recording electrode were placed in a Faraday cage to reduce the background noise. Voltage signals from the electrodes were preamplified with a Neuroprobe Amplifier Model 1600 (A-M Systems) and further amplified with a differential amplifier (custom-made). Both amplifiers were operated in DC mode with 10× and 50× gain, respectively. The amplified signals were displayed on an analog oscilloscope (HAMEG Instruments) via a DS1M12 Pocketscope (Meilhaus Electronic) on the PC using the data-logging software EasyLogger (Meilhaus Electronic). A halogen lamp (Spindler & Hoyer) was used for the generation of white light. The light beam passed through a KG heat filter (Schott), an electronic shutter (Melles Griot), and a plano-convex lens. The lens focused the light beam on a quartz glass fiber (LOT-Oriel) that transferred the light to the fly. Neutral density filters (Schott) were used to attenuate the light intensity. Light intensity was measured at the position of the fly with the QE6500 spectrometer (Ocean Optics). The maximum light intensity was 9.75×10^{14} photons·cm^{-2}·s^{-1}. Before the start of each experiment, flies were dark-adapted for 15 min. Light stimuli of 400-ms duration and different intensities were applied with an interstimulus interval of 20 s to keep the flies in a reasonably dark-adapted state. Experiments were run starting with the lowest light intensity to minimize adaptation effects.

Analysis. The receptor-potential amplitudes of the electroretinogram (ERG) responses to nine different intensities were plotted as a function of the related light intensity for ZT6, ZT12, ZT18, and ZT24 to yield the irradiance response curves. Each curve was obtained from n = 9–13 flies. Afterward, the photon flux needed to elicit a criterion response of 6 mV was determined for each ZT. Finally, the reciprocal of the photon flux was normalized to the according mean value at ZT6 and plotted as a function of the related ZT to yield the circadian fluctuations in ERG sensitivity.

Optomotor Activity Test. ***Setup 1.*** The walking optomotor test was performed as in ref. 37. Specifically, 3- to 8-d-old flies (entrained in a 12:12 light:dark cycle) were placed in a T-shaped tube with the longer arm painted black, located in the center of an arena inside a rotating drum, and tested between ZT1 and ZT4 (Fig. S4*A*) or ZT6 and ZT18 (Fig. 4*C*) . The internal walls of the drum were painted with alternating black and white stripes, and the apparatus was illuminated from above with a white light (2,000 lx). Attracted by the light, tested flies exited the darkened arm of the T tube and were then exposed to the black-and-white rotating drum. Normal flies tend to move in the same direction as the rotating environment. The test was repeated 10 times for each fly: 5 times with clockwise and 5 times with counterclockwise rotations randomly distributed. Each fly was thus scored for the number of correct turns taken in the 10 trials.

Setup 2. Five- to six-day-old flies were starved for 3 h before the experiments to increase the general activity level. Between ZT11 and ZT12 (Fig. S4*B*), when flies are usually active, or at ZT6 and ZT18 (Fig. 4*B*), single flies were put into a walking chamber (circular arena: Ø 3 cm; height: 0.15 cm) in the center of a transparent Plexiglas cylinder (Ø 3.4 cm; height: 1.5 cm), which was placed in the middle of an upright cylinder (Ø 8 cm; height: 4.5 cm). The walls of the outer cylinder were covered with six equally spaced vertical black stripes (width: 30°). Hence, the outer cylinder constitutes a striped drum with a pattern wavelength of λ = 60°, which was rotated around the arena with an angular velocity of ω= 60°/s (10 revolutions per minute). Accordingly, the effective optomotor stimulus was given by a contrast frequency of ω/λ = 1 Hz. The illumination was provided by a ring of white light-emitting diodes (LEDs) surrounding the striped drum (Ø = 19 cm; n = 15 LEDs; light intensity in the center of the striped drum = 23 μW/cm^2). Before the experiment, the flies were dark-adapted for 10 min. For recording of the optomotor response (OR), the cylinder was rotated clockwise (cw) for 5 min and then counterclockwise (ccw) for another 5 min. Between cw and ccw rotation, a darkness period of 5-s duration was inserted. The optomotor response was calculated as $OR = (rev_{cw} + rev_{ccw})/(n_{cw}+n_{ccw}) \times 100\%$, where rev_{cw} indicates the observed number of cw revolutions of the fly during the first 5 min, rev_{ccw} the observed number of the fly's ccw revolutions during the second 5 min, n_{cw} and n_{ccw} are the numbers of revolutions of the striped drum during the cw and ccw periods, respectively. Please note that in this paradigm a result of "OR = 0%" would indicate "no optomotor response" (completely motion-blind flies), whereas, in contrast, a result of "0%" in setup 1 would indicate "100% wrong choice," which would be interpreted as a 100% negative optomotor response. For each genotype, 32 flies were tested at ZT 11–12.

Phototaxis. The light source for the experiment was a fluorescent lamp (intensity of the light at the apparatus: ~3,000 lx). The experiment consisted of five cycles, whereby the flies were able to run from one tube into another for 15 s. At the end, the flies were distributed within six tubes. By counting the number of flies in the different tubes, a performance index was calculated with 0 meaning "no fly showed phototaxis" and 1 meaning "all flies showed phototaxis five times." For each genotype, about 400 flies were tested.

Statistical Analysis. All of the results were expressed as means ± SEM. Data were tested for normal distribution using the Kolmogorov–Smirnov test and further compared by ANOVA, unpaired Student t test, or Mann–Whitney U test to determine significant differences (SYSTAT 11). P values <0.05 were considered statistically significant. Bonferroni's Multiple Comparison test was applied for post hoc comparison.

1. Kimple ME, Siderovski DP, Sondek J (2001) Functional relevance of the disulfide-linked complex of the N-terminal PDZ domain of InaD with NorpA. *EMBO J* 20(16): 4414–4422.
2. Mishra P, et al. (2007) Dynamic scaffolding in a G protein-coupled signaling system. *Cell* 131(1):80–92.
3. Songyang Z, et al. (1997) Recognition of unique carboxyl-terminal motifs by distinct PDZ domains. *Science* 275(5296):73–77.
4. Wes PD, et al. (1999) Termination of phototransduction requires binding of the NINAC myosin III and the PDZ protein INAD. *Nat Neurosci* 2(5):447–453.
5. Tsunoda S, et al. (1997) A multivalent PDZ-domain protein assembles signalling complexes in a G-protein-coupled cascade. *Nature* 388(6639):243–249.
6. Shieh BH, Zhu MY, Lee JK, Kelly IM, Bahiraei F (1997) Association of INAD with NORPA is essential for controlled activation and deactivation of Drosophila phototransduction in vivo. *Proc Natl Acad Sci USA* 94(23):12682–12687.
7. van Huizen R, et al. (1998) Two distantly positioned PDZ domains mediate multivalent INAD-phospholipase C interactions essential for G protein-coupled signaling. *EMBO J* 17(8):2285–2297.
8. Xu XZ, Choudhury A, Li X, Montell C (1998) Coordination of an array of signaling proteins through homo- and heteromeric interactions between PDZ domains and target proteins. *J Cell Biol* 142(2):545–555.
9. Smith DP, et al. (1991) Photoreceptor deactivation and retinal degeneration mediated by a photoreceptor-specific protein kinase C. *Science* 254(5037):1478–1484.
10. Montell C (2007) Dynamic regulation of the INAD signaling scaffold becomes crystal clear. *Cell* 131(1):19–21.
11. Kumar R, Shieh BH (2001) The second PDZ domain of INAD is a type I domain involved in binding to eye protein kinase C. Mutational analysis and naturally occurring variants. *J Biol Chem* 276(27):24971–24977.

12. Shieh BH, Zhu MY (1996) Regulation of the TRP Ca2+ channel by INAD in Drosophila photoreceptors. *Neuron* 16(5):991–998.
13. Szklarczyk D, et al. (2011) The STRING database in 2011: Functional interaction networks of proteins, globally integrated and scored. *Nucleic Acids Res* 39(Database issue):D561–D568.
14. Letunic I, Doerks T, Bork P (2009) SMART 6: Recent updates and new developments. *Nucleic Acids Res* 37(Database issue):D229–D232.
15. Walsh I, et al. CSpritz: Accurate prediction of protein disorder segments with annotation for homology, secondary structure and linear motifs *Nucleic Acids Res* 39(Web Server issue):W190-W196.
16. Gould CM, et al. (2010) ELM: The status of the 2010 eukaryotic linear motif resource. *Nucleic Acids Res* 38(Database issue):D167–D180.
17. Larkin MA, et al. (2007) Clustal W and Clustal X version 2.0. *Bioinformatics* 23(21): 2947–2948.
18. Tamura K, et al. (2011) MEGA5: Molecular evolutionary genetics analysis using maximum likelihood, evolutionary distance, and maximum parsimony methods. *Mol Biol Evol* 28(10):2731–2739.
19. Finn RD, et al. (2010) The Pfam protein families database. *Nucleic Acids Res* 38 (Database issue):D211–D222.
20. Albrecht M, Tosatto SC, Lengauer T, Valle G (2003) Simple consensus procedures are effective and sufficient in secondary structure prediction. *Protein Eng* 16(7):459–462.
21. Berman H, Henrick K, Nakamura H, Markley JL (2007) The worldwide Protein Data Bank (wwPDB): Ensuring a single, uniform archive of PDB data. *Nucleic Acids Res* 35(Database issue):D301–D303.
22. Bindewald E, Cestaro A, Hesser J, Heiler M, Tosatto SC (2003) MANIFOLD: Protein fold recognition based on secondary structure, sequence similarity and enzyme classification. *Protein Eng* 16(11):785–789.
23. Tosatto SC, Bindewald E, Hesser J, Männer R (2002) A divide and conquer approach to fast loop modeling. *Protein Eng* 15(4):279–286.
24. Van Der Spoel D, et al. (2005) GROMACS: Fast, flexible, and free. *J Comput Chem* 26(16):1701–1718.
25. Benkert P, Schwede T, Tosatto SC (2009) QMEANclust: Estimation of protein model quality by combining a composite scoring function with structural density information. *BMC Struct Biol* 9(1):35.
26. Benkert P, Tosatto SC, Schomburg D (2008) QMEAN: A comprehensive scoring function for model quality assessment. *Proteins* 71(1):261–277.
27. Vanin S, et al. (2012) Unexpected features of Drosophila circadian behavioural rhythms under natural conditions. *Nature* 484(7394):371–375.
28. Tsunoda S, et al. (1997) A multivalent PDZ-domain protein assembles signalling complexes in a G-protein-coupled cascade. *Nature* 388(6639):243–249.
29. Porter JA, Hicks JL, Williams DS, Montell C (1992) Differential localizations of and requirements for the two Drosophila ninaC kinase/myosins in photoreceptor cells. *J Cell Biol* 116(3):683–693.
30. Dolezelova E, Dolezel D, Hall JC (2007) Rhythm defects caused by newly engineered null mutations in Drosophila's cryptochrome gene. *Genetics* 177(1):329–345.
31. Busza A, Emery-Le M, Rosbash M, Emery P (2004) Roles of the two Drosophila CRYPTOCHROME structural domains in circadian photoreception. *Science* 304(5676): 1503–1506.
32. Emery P, So WV, Kaneko M, Hall JC, Rosbash M (1998) CRY, a *Drosophila* clock and light-regulated cryptochrome, is a major contributor to circadian rhythm resetting and photosensitivity. *Cell* 95(5):669–679.
33. Dissel S, et al. (2004) A constitutively active cryptochrome in *Drosophila melanogaster*. *Nat Neurosci* 7(8):834–840.
34. Wilm M, et al. (1996) Femtomole sequencing of proteins from polyacrylamide gels by nano-electrospray mass spectrometry. *Nature* 379(6564):466–469.
35. Golemis EA, Brent R (1997) Searching for interacting proteins with the two-hybrid system III. *The Yeast Two-Hybrid System*, eds Bartel PL, Field S (Oxford University Press, New York), pp 43–72.
36. Ausbel FM (1998) *Current protocols in molecular biology* (Green Publishing Associated, New York).
37. Zordan MA, et al. (2006) Post-transcriptional silencing and functional characterization of the *Drosophila melanogaster* homolog of human *Surf1*. *Genetics* 172(1):229–241.

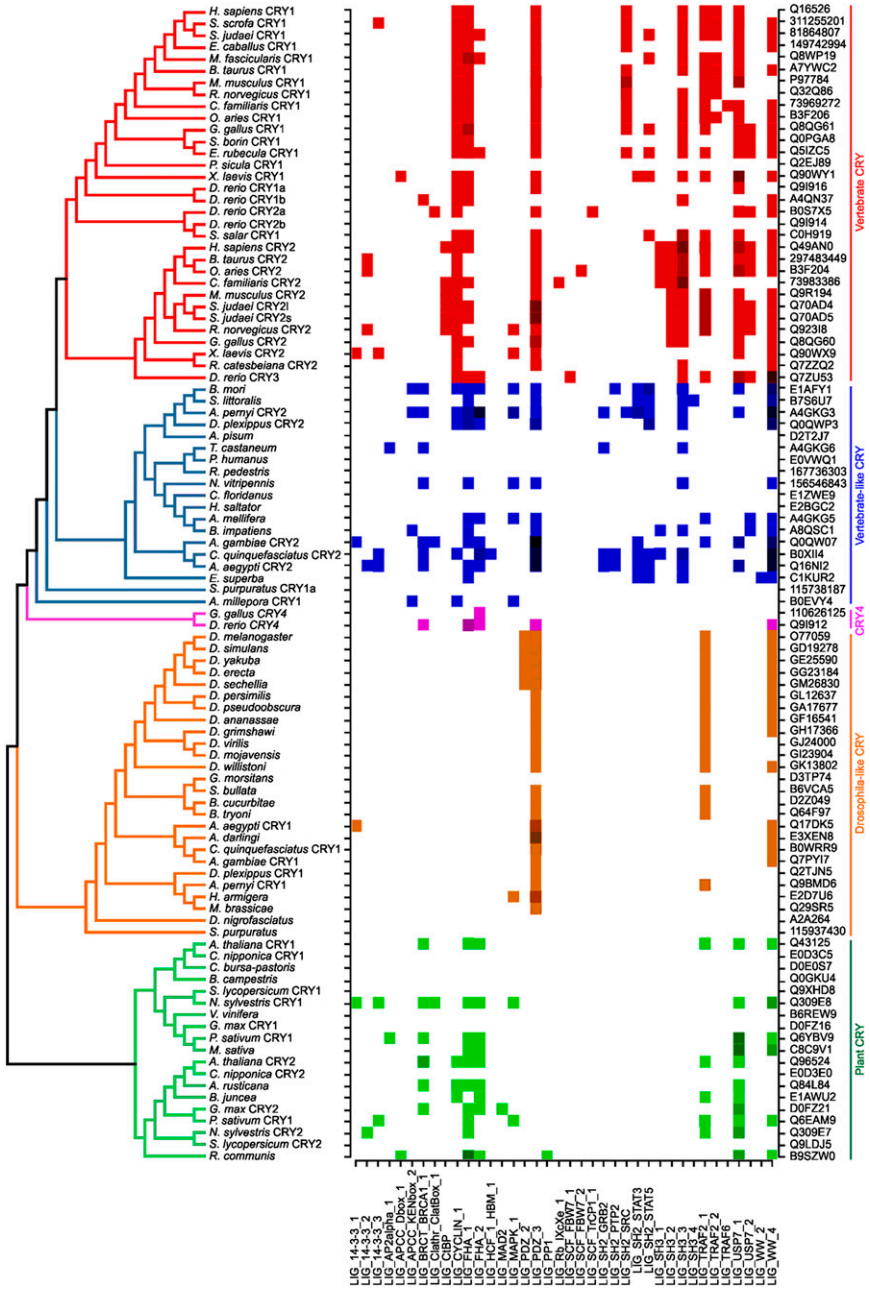

Fig. S1. Distribution of functional motifs in CRY across species. The neighbor-joining phylogenetic tree of 98 known CRY and CRY-like proteins is shown (*Left*) for the N-terminal photolyase-like domain and related to the presence of several functional motifs (identified in the highly variable C terminus) through colored squares (*Center*). The functional motifs are taken from ELM, limited to true binding motifs, and listed with their names on the bottom row. UniProt sequence accession numbers are shown on the *Right* with the high-level taxonomic grouping of the sequences. The latter is also used to color both the phylogenetic tree and the *Center* boxes. Note that darker box colors correspond to more motifs of the same type found in the sequence. The presence of long vertical stripes indicates the evolutionary conservation of a particular functional motif, with the class III PDZ-binding motif corresponding to the longest of such stripes. This is of particular relevance, given the potentially high error rate of single-motif instances.

A

Gel band	Acc. No.	MM (Da)	Protein name	Sequences of the tryptic peptides
RDGA (~ 115 kDa)[a]	Q09103-3	115,579 (Isoform B)[b]	Retinal DeGeneration A protein (RDGA)	GDVQVNPLEK FEESISYPK QVFDLTQGGPK ALGWGGGYTDEPIGK NANEIATYLESQER AFIVKPIPSPEVIPVIVFINPK
NINAC (~ 180 kDa)[a]	P10676	174,300 (Isoform B, long form) 131,836 (Isoform A, short form)	Neither Inactivation Nor Afterpotential protein C (NINAC)	ALGVLDTVIAR[c]

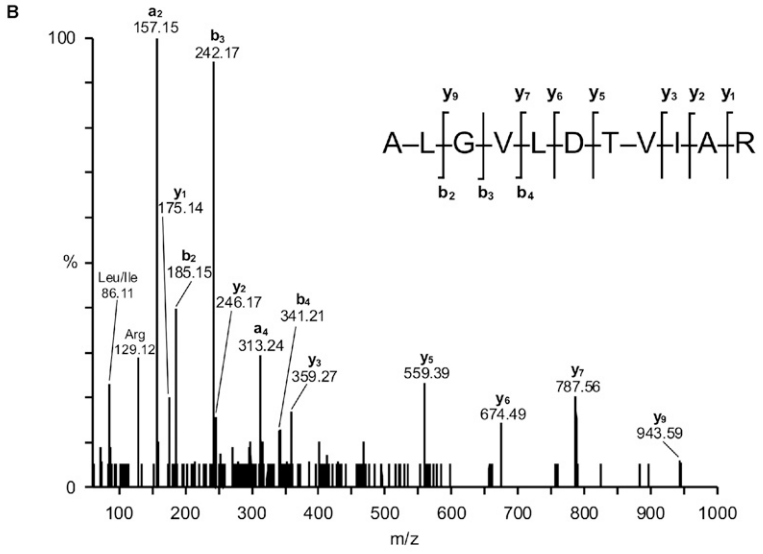

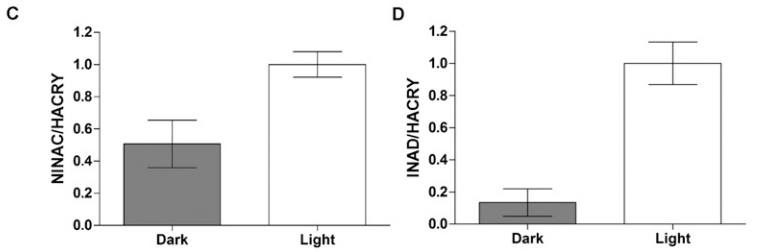

Fig. S2. Proteins identified by LC-MS/MS and quantification of dCRY in the phototransduction complex. (*A*) [a]For the electrophoretic bands corresponding to RDGA and NINAC (Fig. 1), the identified proteins with their accession numbers and molecular masses (MM) are listed. Protein identification was performed with the MASCOT software searching LC-MS/MS data against the sequences of *Drosophila* in the Swiss-Prot database. The fifth column contains a list of the peptides that were sequenced by MS/MS. [b]The peptide sequence NANEIATYLESQER is present only in isoform B of RDGA. [c]In the case of the band corresponding to NINAC, only one peptide sequenced by LC-MS/MS matched the protein with a significant score. The MS/MS spectrum of this peptide is reported in *B*. (*B*) MS/MS spectrum of the doubly charged ion at 564.39 *m/z*. A database search using MASCOT associated this MS/MS spectrum with a significant score to the tryptic peptide ALGVLDTVIAR of the protein NINAC (*Drosophila melanogaster*). In the mass spectrum, the **y**, **b**, and **a** ions are indicated. The corresponding localization of the product fragments **y** and **b** in the sequence of the peptide is also shown. (*C* and *D*) The interaction of NINAC (*C*) and INAD (*D*) for dCRY at ZT24 (dark) and after 15 min of light was quantified as the ratio NINAC/HACRY and INAD/HACRY, respectively. Mean levels normalized to values obtained after 15 min of light ± SEM of three replicates are shown. The differences between NINACp174/HACRY and INAD/HACRY ratios under light and dark conditions were significant ($P < 0.03$ and $P < 0.02$, respectively, Mann–Whitney *U* test).

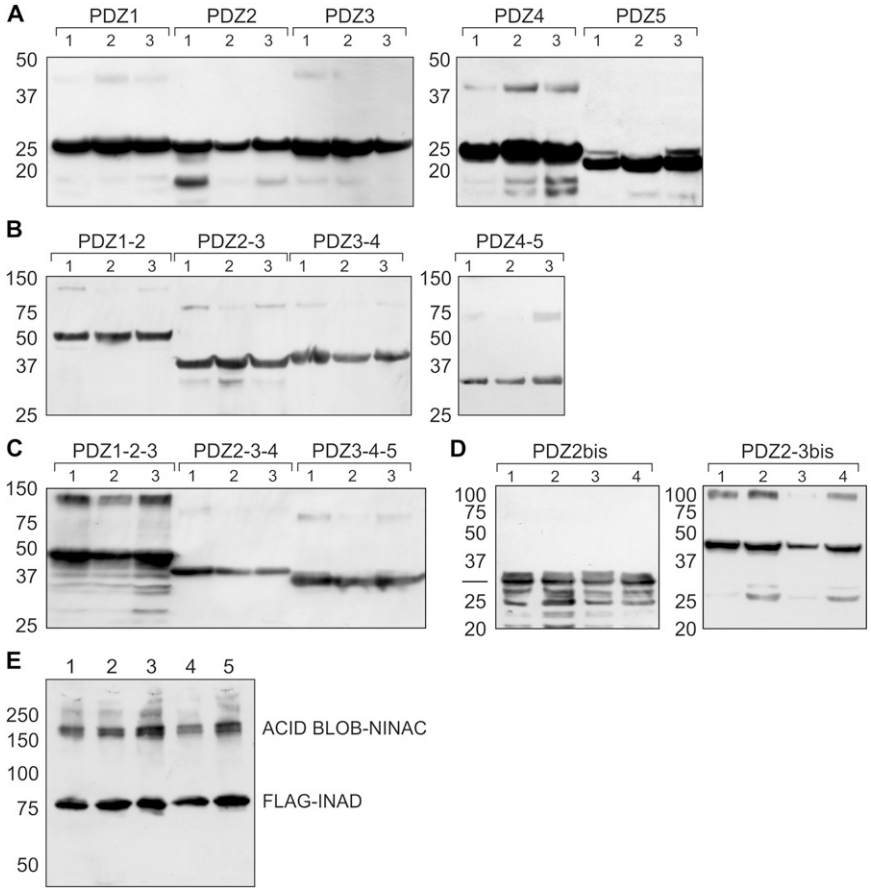

Fig. S3. Western blot analysis of independent yeast clones for prey fusions expressing different combinations of PDZ domains or NINAC as prey fusion and INAD in the nucleus. Three or four independent yeast clones for each prey fusion were probed with anti-HA antibody (Sigma; 1:5,000). The signals corresponding to the fusions are shown. See Table S3 for expected molecular masses. Images originating from different films have been reported in separate panels. (*A*) Single PDZs. The ~20- to 25-kDa signals indicate that all of the fusions are expressed in yeast cells and the absence of interaction cannot be explained by the absence of expression. A band of molecular mass compatible with a dimer is visible in the PDZ1, PDZ3, and PDZ4 lanes. (*B*) Tandem PDZs. (*C*) Three PDZs. All of the fusions are correctly expressed in yeast cells, and traces of dimerization are visible in all of the combinations. (*D*) Extended version of PDZ2 and PDZ2–3 tandem, including the CaM motif upstream from the canonical PDZ2 boundary. (*E*) Independent yeast clones expressing dCRY as bait, NINAC as prey (AcidBlob-NinaC) and a FLAG-tagged form of INAD specifically in the yeast nucleus were probed with anti-HA and anti-FLAG antibodies. The signals corresponding to the expressed fusions are shown.

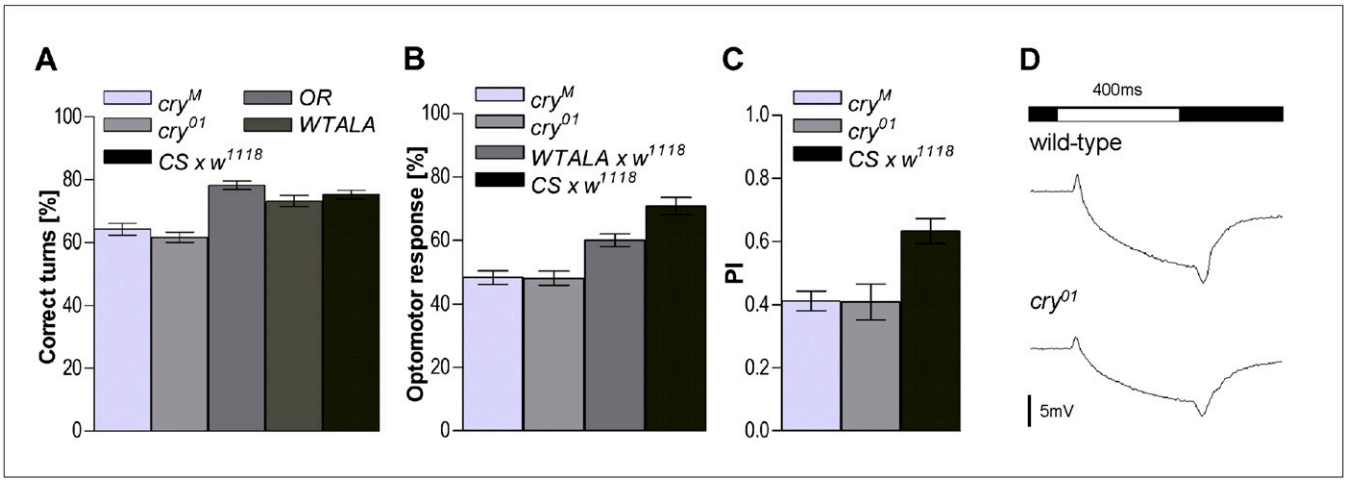

Fig. S4. Visual behavior of dCRY mutants. (*A*) Percentage of correct choices with respect to the direction of the stripe motion (optomotor stimulus) inside a T-shaped tube (setup 1, *SI Materials and Methods*). Male cry^{M}, cry^{01}, Oregon R, WT-Alto Adige (ALA), and CS × w^{1118} flies (100 for each genotype) were analyzed between ZT1 and ZT4. cry^{01} and cry^{M} exhibited 61.6 and 64.2% of correct turns, respectively, whereas wild-type controls (Oregon R, WT-ALA, and the progeny of a CS × w^{1118} cross) achieved 78.2, 73.2, and 75.2%, respectively. Mean values ± SEM are given. Both cry^{01} and cry^{M} displayed an impairment in their optomotor turning response with respect to controls ($F_{4,495} = 19.53$, $P < 0.0001$). No difference was found between the two *cry* mutants ($P > 0.05$). (*B*) Optomotor response for cry^{M}, cry^{01}, WT-ALA × w^{1118}, and CS × w^{1118} males, with setup 2 (*SI Material and Methods*). The mean optomotor response of single flies placed in a Plexiglas arena is expressed as the percentage of fly revolutions with respect to the number of revolutions of the optomotor stimulus (striped drum). Both cry^{01} and cry^{M} mutants showed an optomotor response (OR) of about 48% whereas control flies (the progeny of CS × w^{1118} and WT-ALA × w^{1118} crosses) showed an OR of about 71 and 60%, respectively. Thirty-two flies for each genotype were analyzed between ZT11 and ZT12. Mean values ± SEM are given. As in setup 1, both *cry* mutant flies showed a reduced optomotor response with respect to the wild-type flies ($F_{3,124} = 22.35$, $P < 0.0001$). Whereas the 50% level in *A* denotes random choice behavior (no optomotor response to the moving stripes), the same value of 50% in *B* would indicate that the fly completed 50% of the revolutions imposed by the rotating striped drum. Therefore, the mutants' OR levels in *B* correspond to about 68–80% of the WT OR. Both optomotor experiments reveal a significant OR reduction in cry^{01} and cry^{M}. (*C*) Phototaxis response for cry^{M}, cry^{01}, and CS × w^{1118}. The performance index (PI) is expressed as the number of times that flies show phototaxis in a five-cycle test, with 0 meaning "no fly showed phototaxis" and 1 meaning "all flies showed phototaxis five times." About 400 flies for each genotype were tested between ZT11 and ZT12. Both cry^{01} and cry^{M} flies showed a significant reduction in the phototactic response with respect to the wild-type flies ($F_{2,26} = 8.2$, $P = 0.002$). (*D*) Electroretinograms of wild-type flies and cry^{01} mutants. cry^{01} mutants exhibit normal, wild-type-like ERG responses upon illumination with white light. The electroretinograms were recorded at ZT18 with white light pulses of 400-ms duration and an intensity (*I*) of 9.75×10^{14} photons·cm^{-2}·s^{-1}.

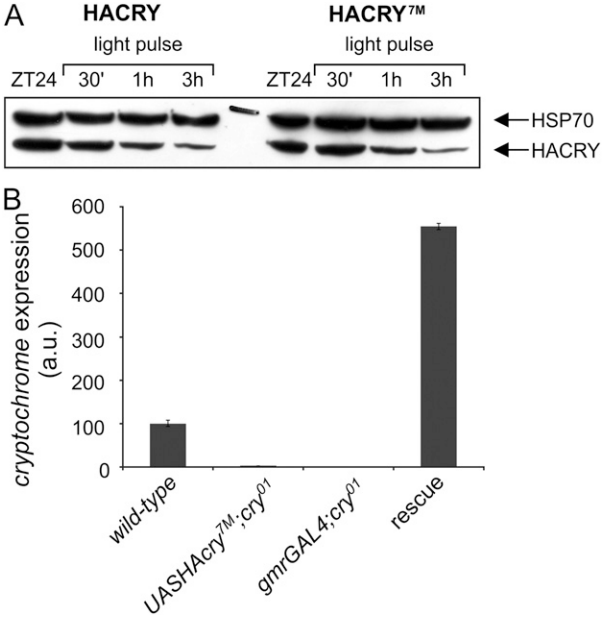

Fig. S5. Molecular characterization of HAcry^{7M} strain. We had previously obtained a *UAS-HAcry*^{7M}, an HA-tagged variant of d*cry* in which a tyrosine (amino acid 497 in the chimeric protein) was substituted with alanine. (*A*) Western blot analysis, performed with anti-HA antibody, showing that the Y497A substitution does not influence the temporal light degradation profile of cryptochrome. *UAS-HAcry*^{7M} flies were crossed with flies carrying the *timGAL4* driver, and the progeny was entrained for 3 d under standard light–dark conditions. Individuals were then collected at ZT24 and after 30 min, 1 h, and 3 h of light exposure. As control, the progeny resulting from *UAS-HAcry* crossed with *timGAL4* were used. The housekeeping protein HSP70 was used as loading control. (*B*) Analysis of cryptochrome expression by quantitative RT-PCR. The expression levels of *cry* were analyzed in the following lines used in rescue experiments: wild type (w^{1118}), *UAS-HAcry*^{7M}*;cry01*, *gmrGAL4;cry01*, and rescue (progeny of the cross *UASHAcry*^{7M}*;cry01* × *gmrGAL4;cry01*).

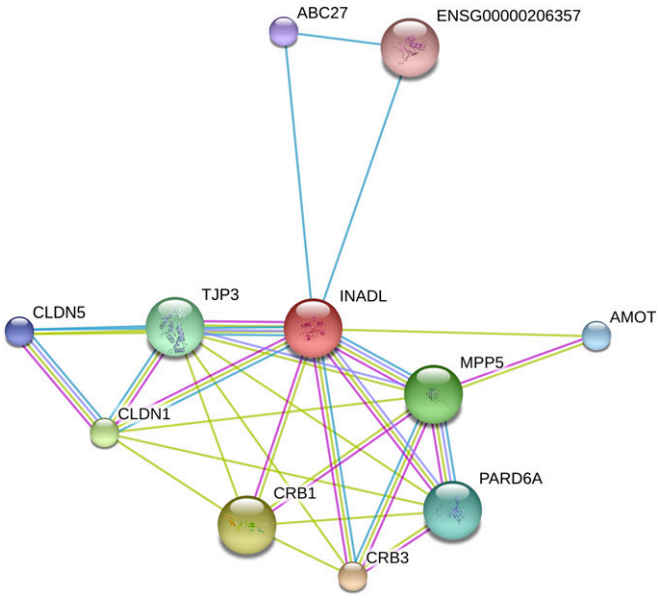

Fig. S6. Protein interaction network surrounding INADL, obtained with the STRING database. Edge colors represent different detection methods.

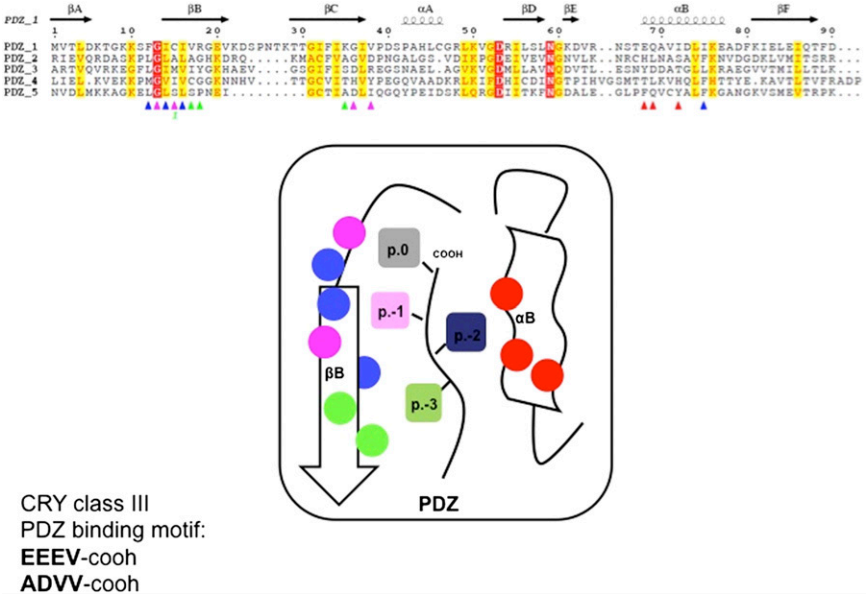

Fig. S7. Specificity determinants of INAD. The sequences of the five INAD PDZ domains are aligned (*Upper*) with the secondary structure elements in canonical nomenclature shown above. Color-coded triangles below the sequences denote the specificity determining residues for PDZ domains, with different colors corresponding to the four main positions on the linear motif counted from the C terminus backward (p.0 through p.-3). The schematic shows the most relevant PDZ secondary structure elements surrounding the linear motif at the center. The positions corresponding to the sequence alignment are colored as follows: gray for p.0, pink for p.-1, blue for p.-2, green for p.-3, and their contacting residues, respectively.

Table S1. Nucleotide sequences and position of primers used

Primer	Length (bp)	Position	Direction	Sequence (5′→3′)
InaD_FL_F	36	1–18	F	CATATGGAATTCGACGTCATGGTTCAGTTCCTGGGC
InaD_FL_R	36	2007–2025	R	TCTAGACTCGAGAAGCTTCTAGGCCTTGGGTGCCTC
InaD_PDZ1_F	36	48–66	F	CATATGGAATTCGACGTCATGGTGACCCTGGACAAG
InaD_PDZ1_R	42	297–318	R	TCTAGACTCGAGAAGCTTCTAGTCGAAGGTCTGAATCTCCAG
InaD_PDZ2_F	36	744–762	F	CATATGGAATTCGACGTCAGGATCGAGGTCCAGAGG
InaD_PDZ2bis_F	42	559–582	F	CATATGGAATTCGACGTCGACGAGGACACCCGGGACATGACC
InaD_PDZ2_R	39	978–996	R	TCTAGACTCGAGAAGCTTCTAGCGTCGCGAGGTGATCAT
InaD_PDZ3_F	36	1080–1098	F	CATATGGAATTCGACGTCTTTCCCAAGGCGCGCACG
InaD_PDZ3_R	45	1311–1335	R	TCTAGACTCGAGAAGCTTCTACAATAGAATCATGGTCACTACGCC
InaD_PDZ4_F	42	1464–1488	F	CATATGGAATTCGACGTCCTCATTGAGTTGAAGGTGGAAAAG
InaD_PDZ4_R	39	1713–1731	R	TCTAGACTCGAGAAGCTTCTAAGGATCAGCGCGGAAGAC
InaD_PDZ5_F	41	1749–1772	F	CATATGGAATTCGACGTCAACGTTGACCTTATGAAAAAAGC
InaD_PDZ5_R	40	1973–1992	R	TCTAGACTCGAGAAGCTTCTACTTGGGTCGTGTCACTTCC
CRYdeltaF	29	1561–1581	F	CCGAATTCCCGCATTGCCGACCATCCAAC
CRYR	33	1604–1629	R	CCCTCGAGTCAAACCACCACGTCGGCCAGCCAG
InaDNLSFLAG_F	112	1–31	F	CCAAGCTTGAATTCATGGATTACAAGGATGACGACGATAAGG GTGCTCCTCCAAAAAAGAAGAGAAAGGTAGCTGGTATCAA TAAAGTTCAGTTCCTGGGCAAACAGGGCACCG
InaDXhoR	31	2006–2025	R	GGTCGACTCGAGCTAGGCCTTGGGTGCCTCC
Nina5F-Sal	32	1–24	F	CCGTCGACATGATGTATTTACCGTACGCGCAA
NinaPB3-Sal	31	4484–4506	R	GGGTCGACTTAGATATCGACGGCATAGCCTG

Position reflects nucleotide location in FlyBase: Fbgn0001263 (INAD), Fbpp0079064 (NINAC), and Fbpp0083150 (dCRY).

Table S2. Expected molecular masses of fusions used in yeast experiments

Fusion (amino acids)	Short name	MM (kDa)
A-inaD (17–106)	PDZ1	21.7
A-inaD (249–332)	PDZ2	20.8
A-inaD (364–448)	PDZ3	20.9
A-inaD (489–577)	PDZ4	21.5
A-inaD (584–664)	PDZ5	20.6
A-inaD (17–332)	PDZ1–2	46.9
A-inaD (249–448)	PDZ2–3	33.1
A-inaD (364–577)	PDZ3–4	35.6
A-inaD (489–664)	PDZ4–5	31.2
A-inaD (207–332)	PDZ2bis	28.2
A-inaD (207–448)	PDZ2-3bis	40.5
A-inaD (17–448)	PDZ1–3	59.2
A-inaD (249–577)	PDZ2–4	47.8
A-inaD (364–664)	PDZ3–5	45.1
A-inaD (1–674)	INAD	86.1
A-NinaC	NINAC	186.1
Nuclear FLAG-inaD (1–674)	NFLAG-INAD	82.1

A, acid blob (prey fusion); MM, molecular mass.